Metal(II) complexes based on 4-(2,6-di(pyridin-4-yl)pyridin-4 -yl)benzonitrile: structures and electrocatalytic properties for hydrogen evolution reaction from water

Xiao Lin Gao,[a] Yun Gong,[*,a] Pan Zhang,[a] Yong Xi Yang, [a] Jiang Ping Meng, [a] Miao Miao Zhang, [a] Jun Li Yin [a] and JianHua Lin[*, a, b]

[a] *Department of Applied Chemistry, College of Chemistry and Chemical Engineering, Chongqing University, Chongqing 400030, P. R. China Tel: +86-023-65106150 E-mail: gongyun7211@cqu.edu.cn*

[b] *Zhejiang University, Hangzhou 310058, P. R. China Tel: +86-0571-88981583 E-mail: jhlin@zju.edu.cn; jhlin@cqu.edu.cn; jhlin@pku.edu.cn*

Determination of Faradaic Efficiency

Controlled potential electrolyses were conducted in a 50 mL 0.5 M Na_2SO_4 solution at an applied potential of □-1.1 V vs SCE (η = -0.46V) for 0.5 hour. The pH change of the solution during the electrolysis was recorded with a pH meter. Assuming 100% Faradaic efficiency, the theoretical pH change over time can be calculated by the equation of pH = 14 + lg {Σ(It)/(FV)}, where I = current (A), t = time (s), F = Faraday constant (96485 C/mol), V = solution volume (0.05 L). [1] The amount of H_2 evolved was determined using gas chromatography (GC, 7890A, thermal conductivity detector (TCD), Ar carrier, Agilent). The theoretical (assuming 100% Faradic efficiency) hydrogen volume is based on the amount of consumed charge during the course of electrolysis.

Table S1 Selected bond lengths (Å) and angles (º) for complexes **1-3**

Complex 1			
Ni(1)-O(5)	1.983(8)	Ni(1)-O(5')	2.191(12)
Ni(1)-O(7)	2.055(3)	Ni(1)-O(6)	2.074(3)
Ni(1)-N(2)	2.123(3)	Ni(1)-N(3)#1	2.124(3)
O(5)-Ni(1)-O(1')	67.5(6)	O(6)-Ni(1)-O(5')	171.3(6)
O(1')-Ni(1)-O(1)	25.52(18)	O(5)-Ni(1)-O(1)	92.6(6)
O(7)-Ni(1)-N(3)#1	86.38(12)	O(1')-Ni(1)-N(3)#1	96.8(2)
O(6)-Ni(1)-N(2)	90.25(14)	N(2)-Ni(1)-N(3)#1	175.24(12)
Complex 2			
Co(1)-O(10)	2.073(4)	Co(1)-O(9)	2.143(4)
Co(2)-O(13)	2.080(4)	Co(2)-O(12)	2.123(4)
Co(1)-N(2)	2.169(4)	Co(1)-N(3)	2.172(5)
Co(2)-N(6)	2.175(4)	Co(2)-N(7)	2.179(4)
O(1)-Co(1)-O(9)	85.07(17)	O(11)-Co(1)-O(1)	178.84(16)
O(14)-Co(2)-O(12)	177.07(16)	O(13)-Co(2)-O(14)	85.60(18)
O(11)-Co(1)-N(3)	85.62(17)	O(1)-Co(1)-N(3)	94.79(17)
O(13)-Co(2)-N(6)	85.77(17)	O(5)-Co(2)-N(6)	95.42(18)
N(2)-Co(1)-N(3)	173.0(2)	N(6)-Co(2)-N(7)	173.6(2)
Complex 3			
Cd(1)-O(10)	2.287(6)	Cd(1)-O(11)	2.349(6)
Cd(2)-O(14)	2.292(7)	Cd(2)-O(12)	2.360(7)

Cd(1)-N(2)	2.330(6)	Cd(1)-N(3)#2	2.335(7)
Cd(2)-N(7)#2	2.342(7)	Cd(2)-N(6)	2.343(7)
O(10)-Cd(1)-O(11)	83.8(2)	O(9)-Cd(1)-O(11)	174.9(2)
O(14)-Cd(2)-O(13)	83.9(3)	O(5)-Cd(2)-O(13)	178.6(2)
O(10)-Cd(1)-N(2)	84.6(2)	O(1)-Cd(1)-N(2)	96.8(3)
O(13)-Cd(2)-N(6)	82.1(2)	O(5)-Cd(2)-N(6)	98.9(2)
N(2)-Cd(1)-N(3)#1	171.1(2)	N(7)#1-Cd(2)-N(6)	166.9(3)

Symmetry transformations used to generate equivalent atoms:

#1 x-1/2, -y+5/2, z-1/2 #2 x+1/2, -y+3/2, z+1/2

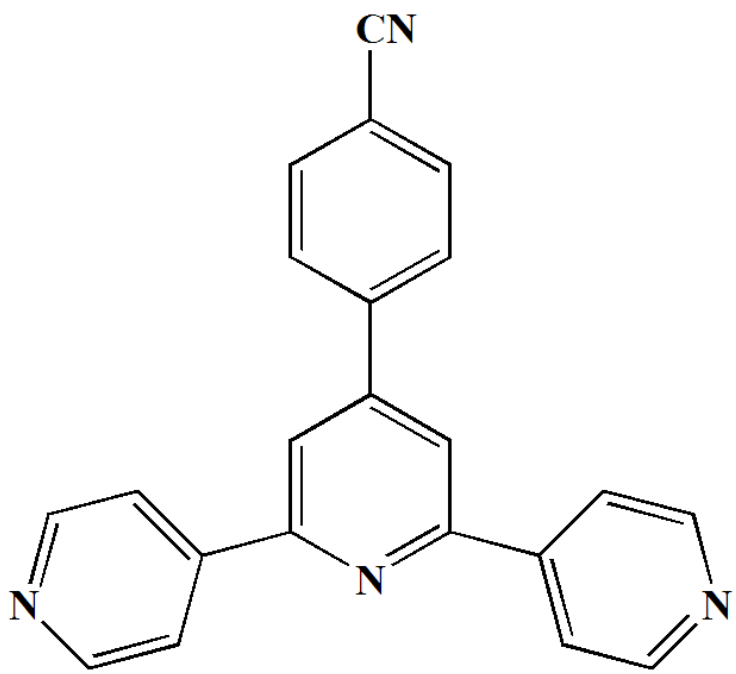

Scheme S1 Schematic representation of **L**

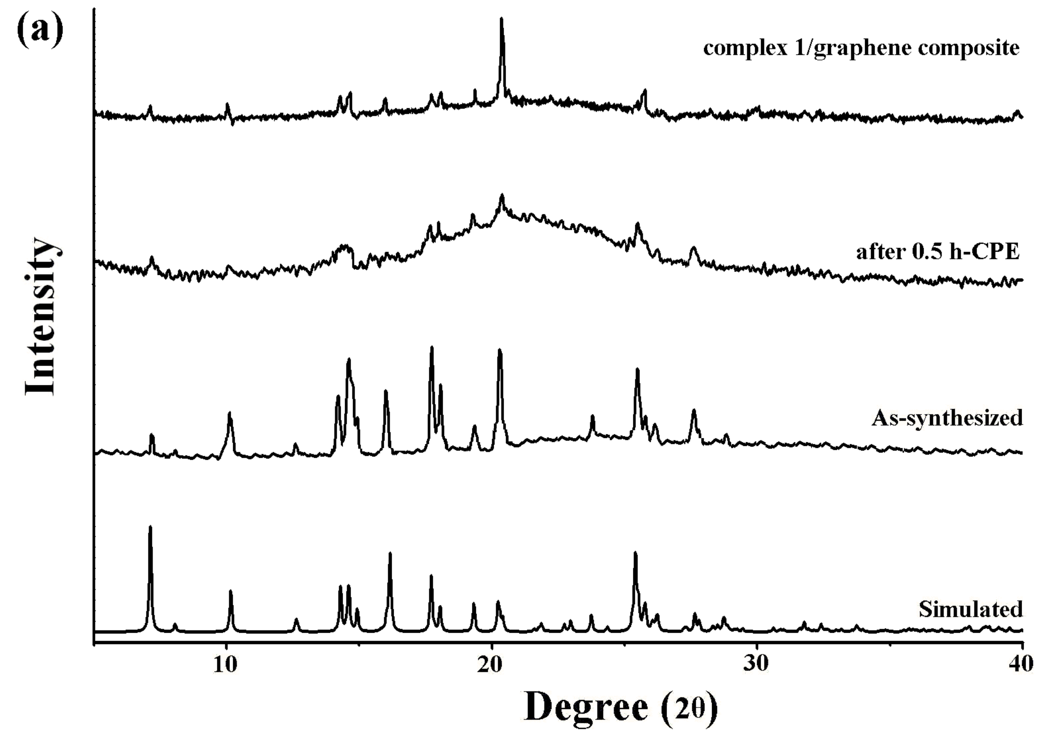
(a)
complex 1/graphene composite
after 0.5 h-CPE
As-synthesized
Simulated
Intensity
10
20
30
40
Degree (2θ)

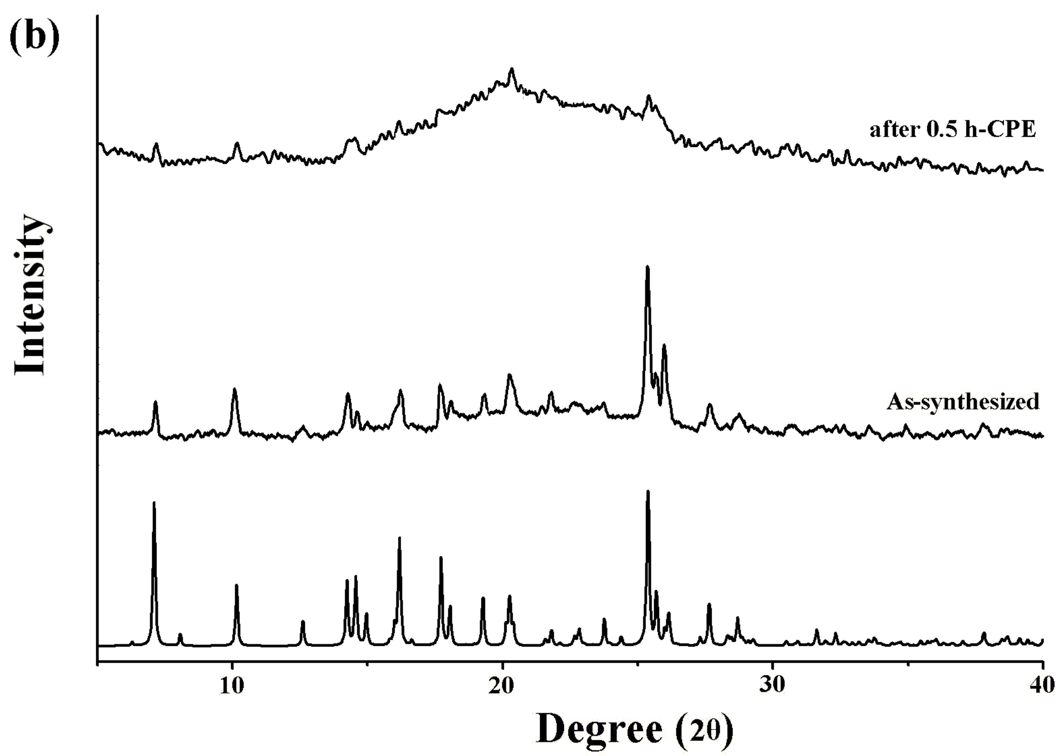
(b)
after 0.5 h-CPE
As-synthesized
Intensity
10
20
30
40
Degree (2θ)

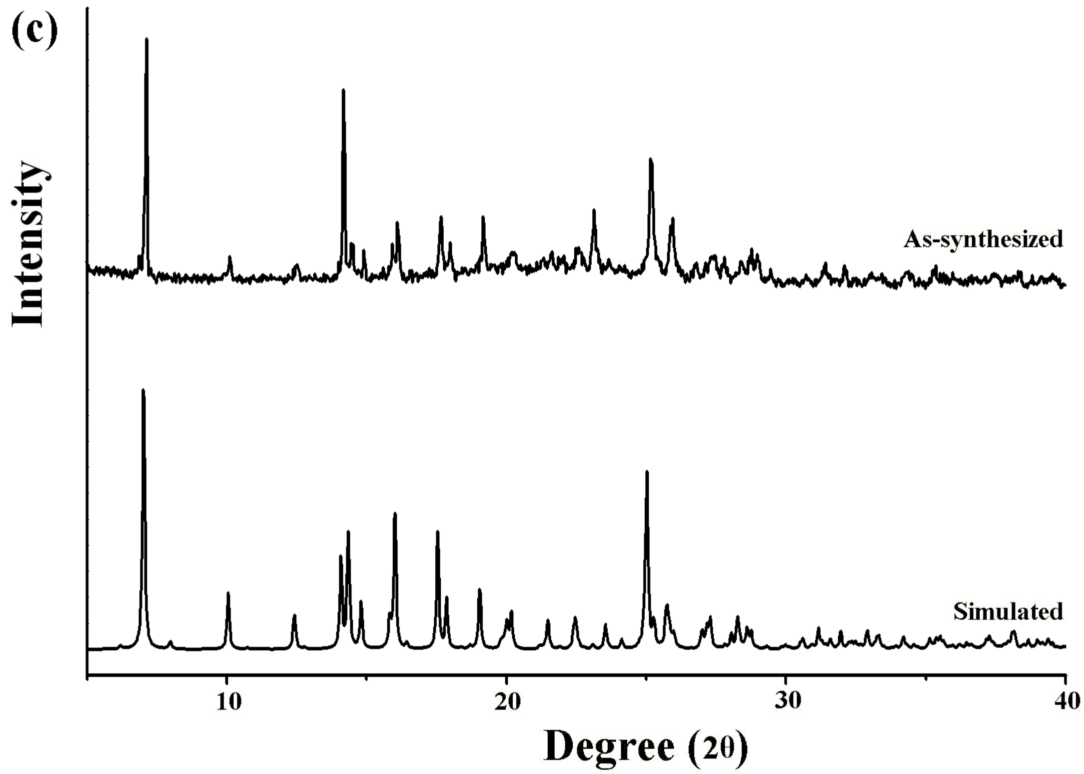

Fig.S1 The powder XRD patterns for complexes **1** (**a**), **2** (**b**) and **3** (**c**).

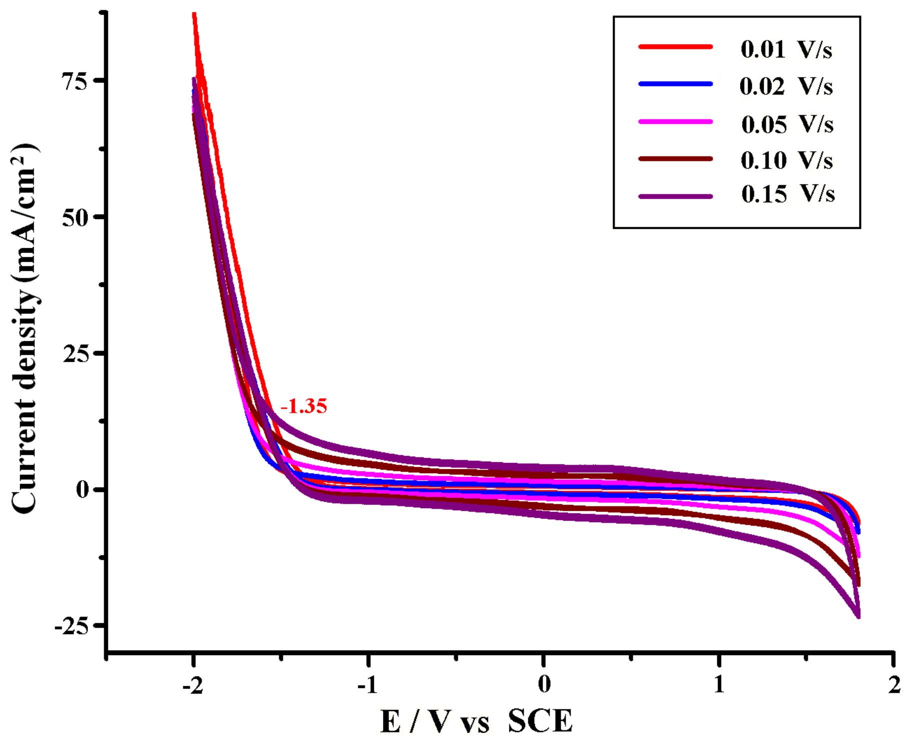

Fig. S2 CVs of the bare **GCE** in the 0.5M Na_2SO_4 aqueous solution (50 mL) at different sweep rates.

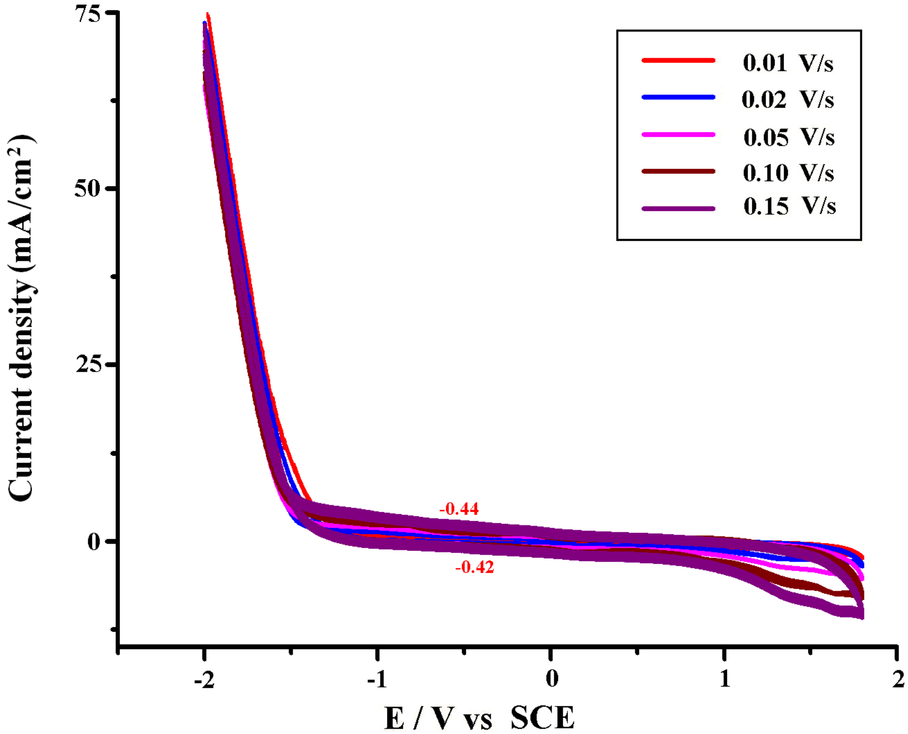

Fig. S3 CVs of the **L-GCE** in the 0.5M Na_2SO_4 aqueous solution (50 mL) at different sweep rates.

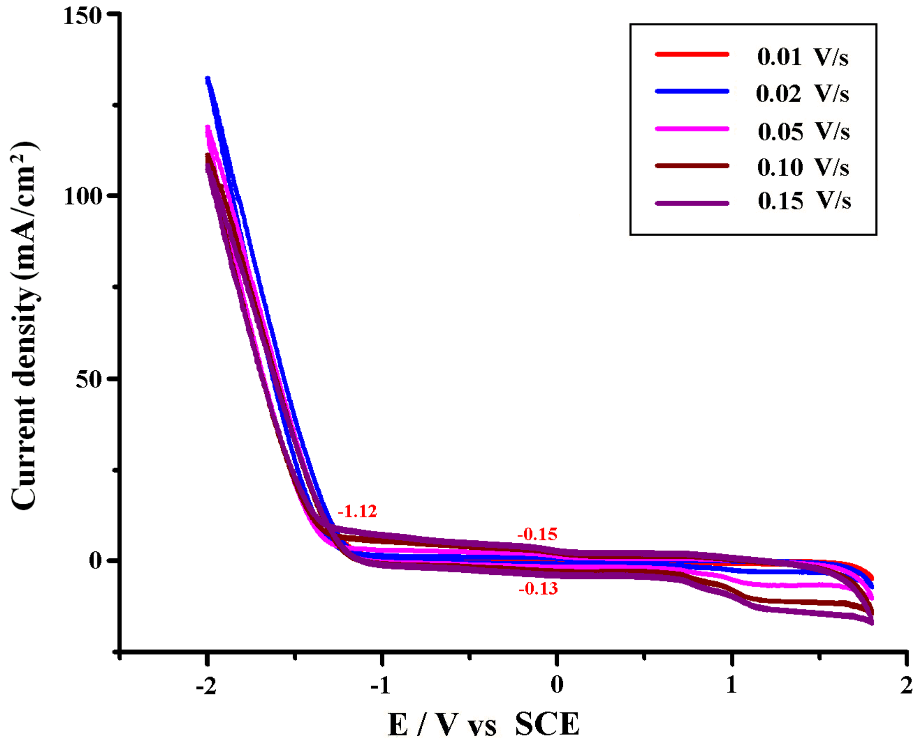

Fig. S4 CVs of the **1-GCE** in the 0.5M Na_2SO_4 aqueous solution (50 mL) at different sweep rates.

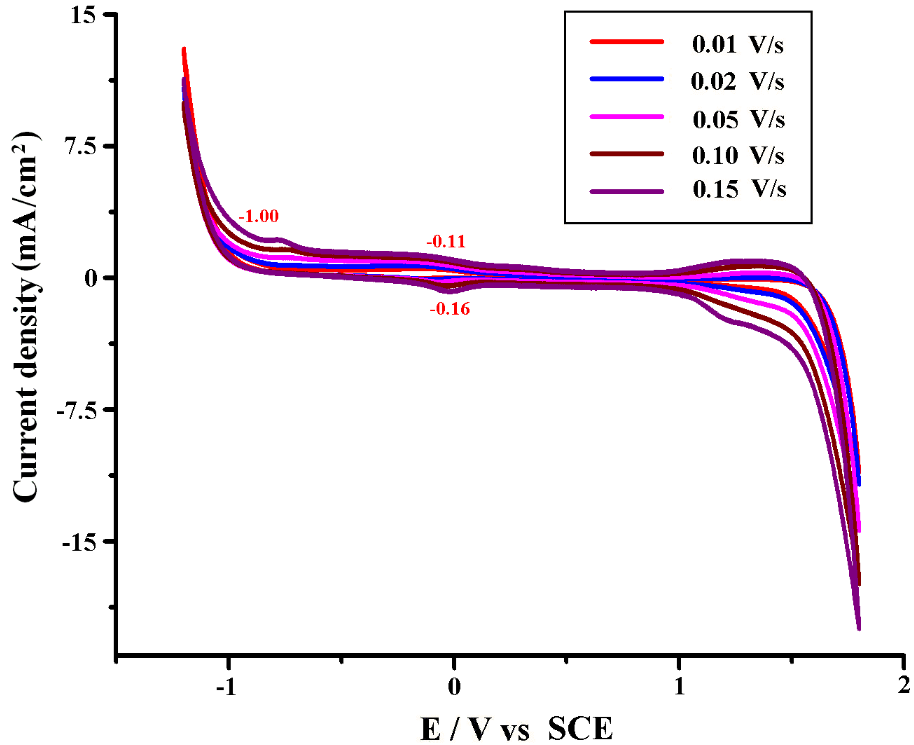

Fig. S5 CVs of the **2-GCE** in the 0.5M Na_2SO_4 aqueous solution (50 mL) at different sweep rates.

(a)

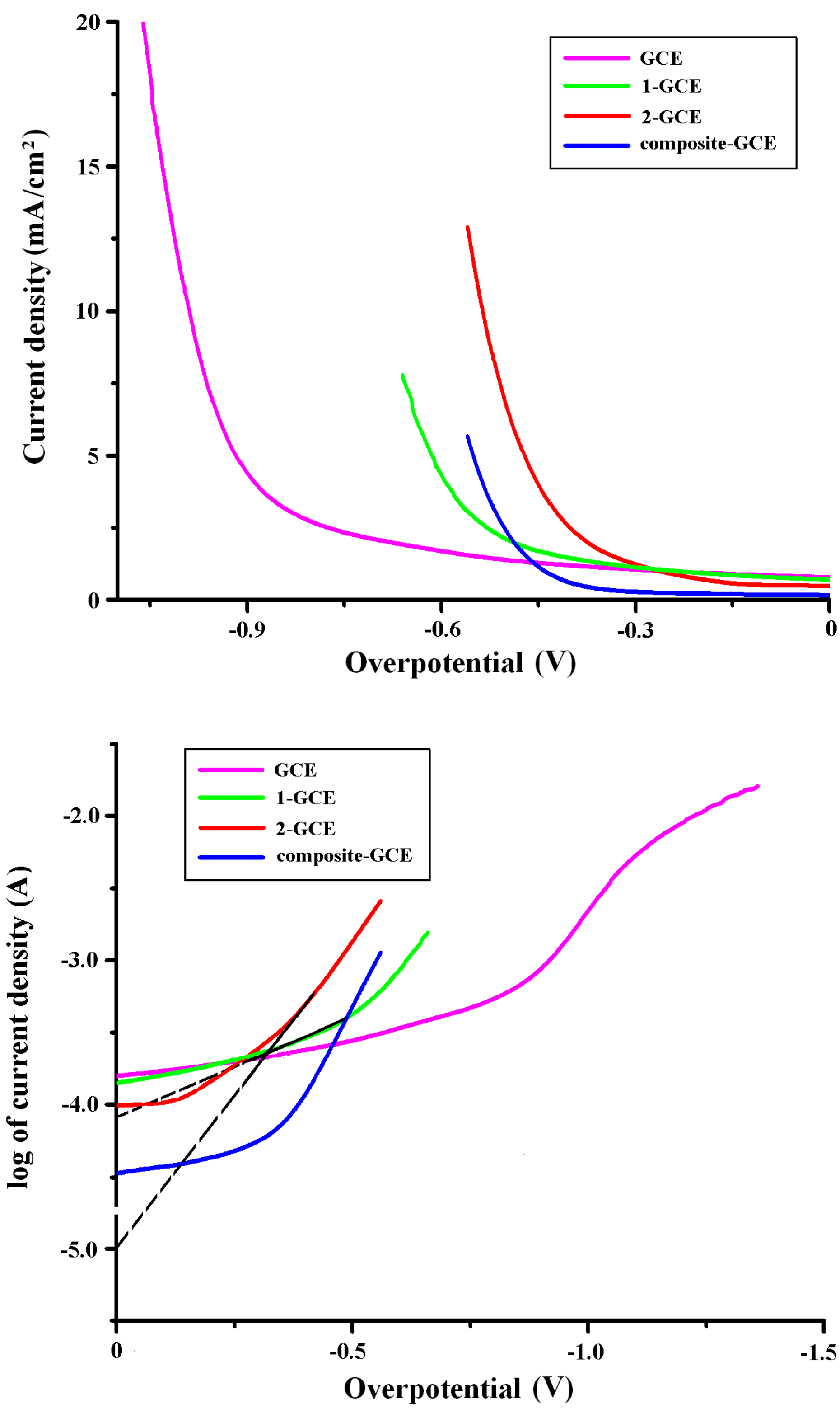

Fig. S6 Current intensity (i) / overpotential (η) diagrams (**a**) for the HER at the bare **GCE**,

1-GCE, **2-GCE** or **composite-GCE** in 0.5 M Na_2SO_4 solution (50mL) at sweep rates of 10 $mV \cdot s^{-1}$; Tafel plots of *logi* against overpotential η for the HER (The linear part of the Tafel curves denoted in black dotted lines with the intercept at the *y* axis) (**b**).

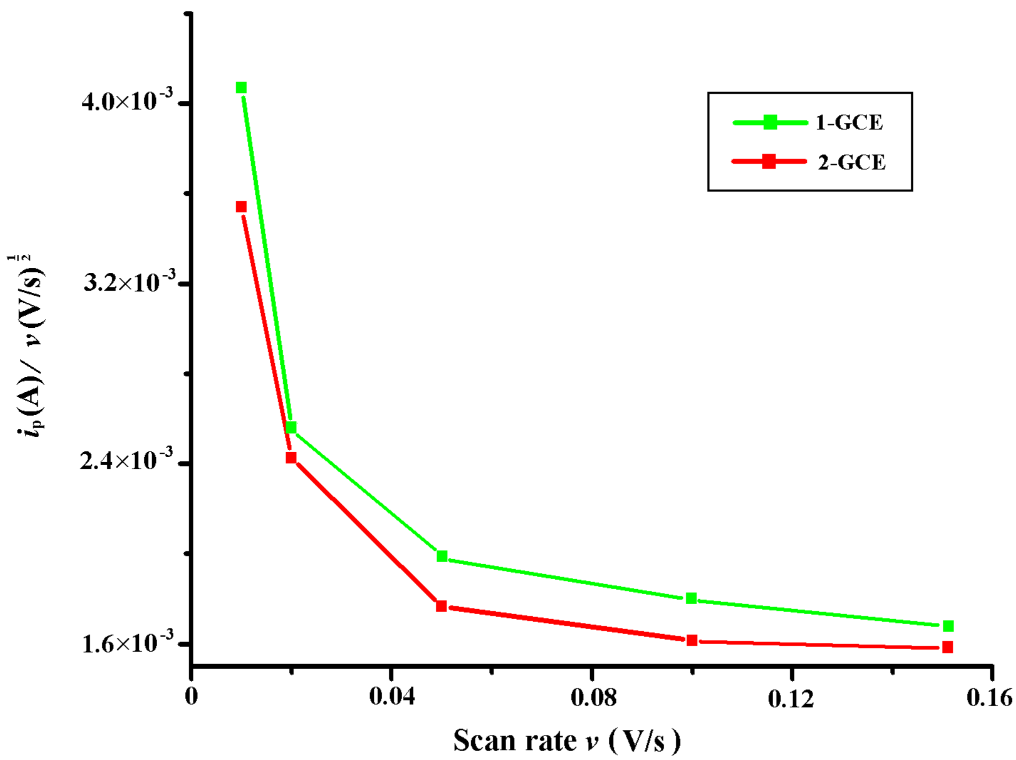

Fig.S7 The plots of i_p / $v^{1/2}$ against scan rate *v*.

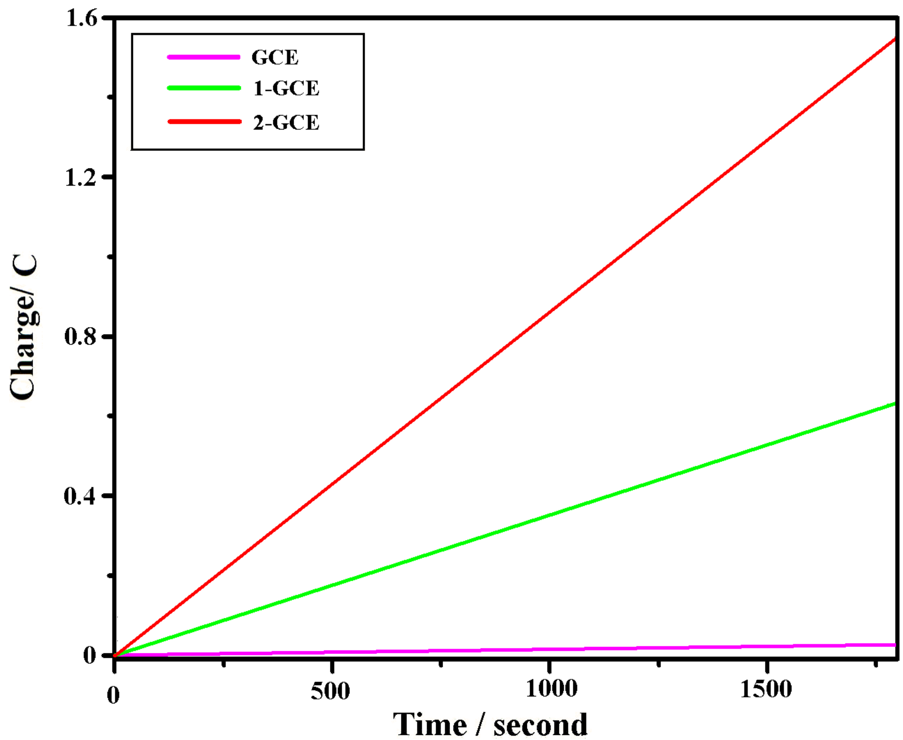

Fig. S8 Controlled potential electrolysis of **1-GCE** (current density = 1.74 mA/cm^2) (green), **2-GCE** (current density = 4.33 mA/cm^2) (red) and the bare **GCE** (current density = 1.34 mA/cm^2) (pink) in the 0.5 M Na_2SO_4 aqueous solution (50mL), showing charge buildup versus time with an applied potential of -1.1V vs SCE (η = -0.44V).

(**a**)

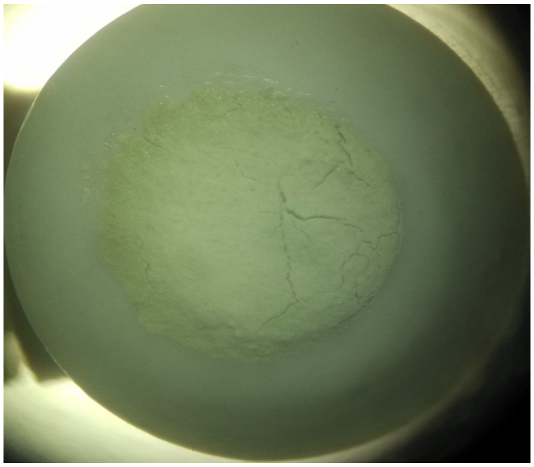

before 0.5 h- electrolysis at -1.1V vs SCE

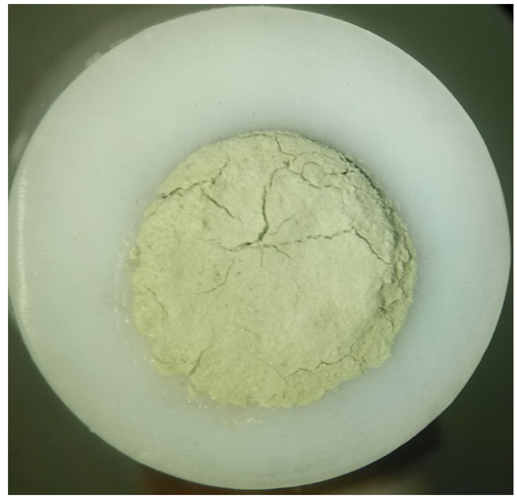

after 0.5 h- electrolysis at -1.1V vs SCE

(**b**)

before 0.5 h- electrolysis at -1.1V vs SCE

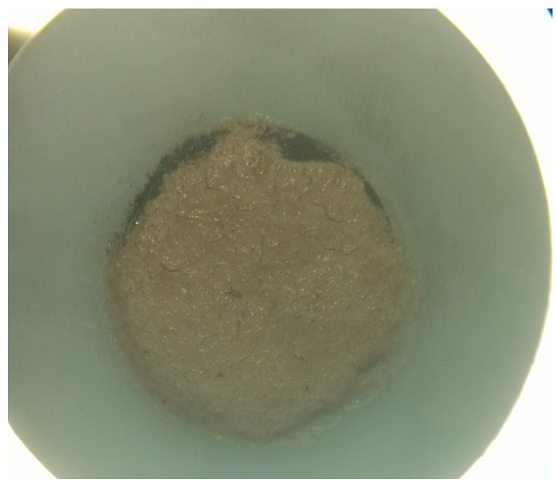

after 0.5 h- electrolysis at -1.1V vs SCE

Fig. S9 The images of **1-GCE** (**a**) and **2-GCE** (**b**) before and after electrolysis at -1.1V vs SCE.

(a)

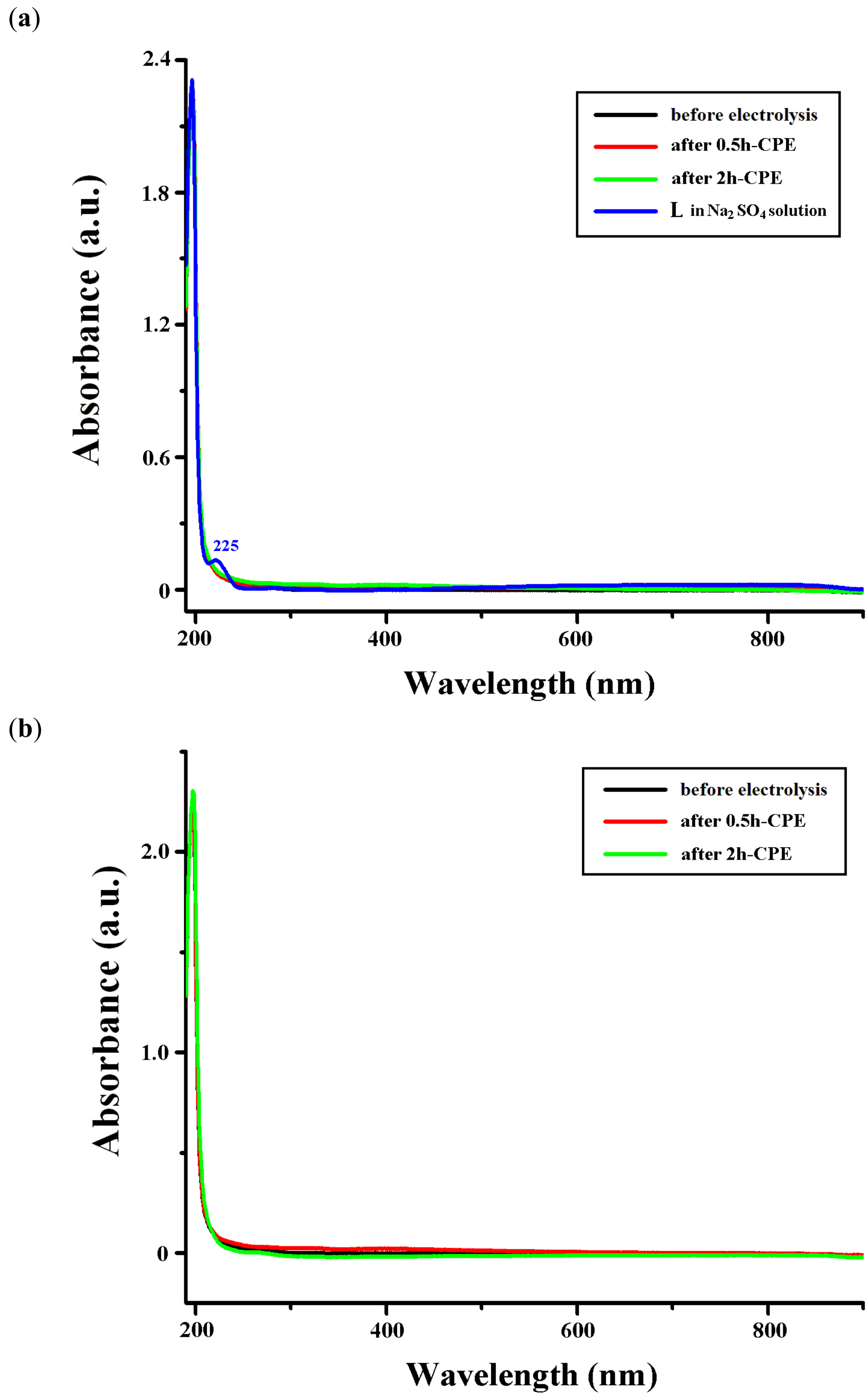

Fig. S10 UV-vis absorption spectra at room temperature for the Na_2SO_4 solution in the presence of **1-GCE** (**a**) or **2-GCE** (**b**) before and after electrolysis at -1.1 V vs SCE.

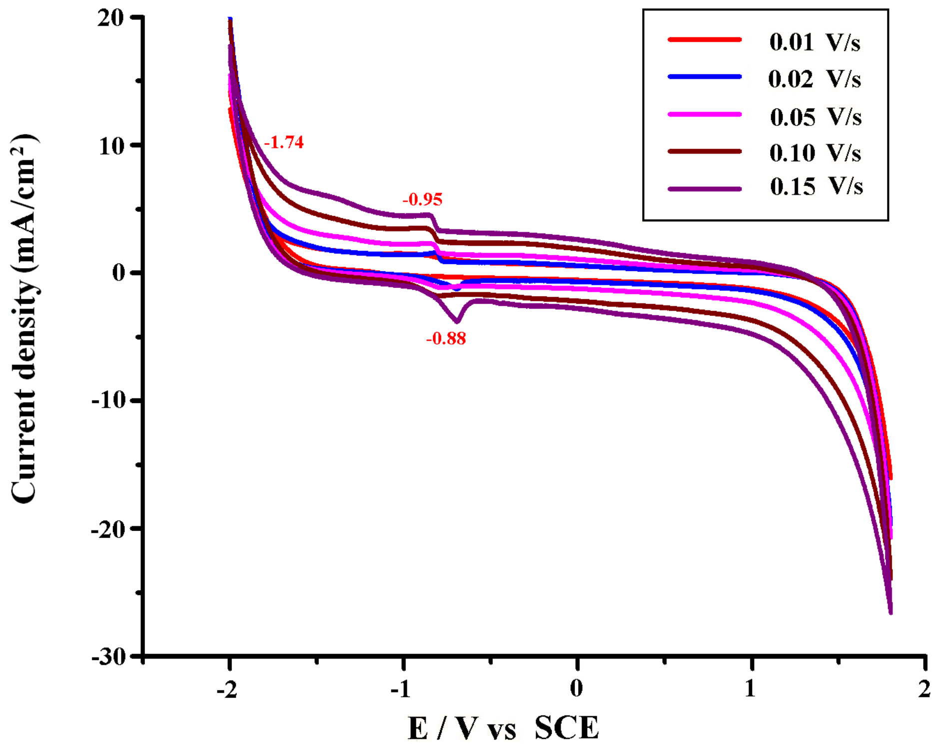

Fig. S11 CVs of the **3-GCE** in the 0.5M Na_2SO_4 aqueous solution (50 mL) at different sweep rates.

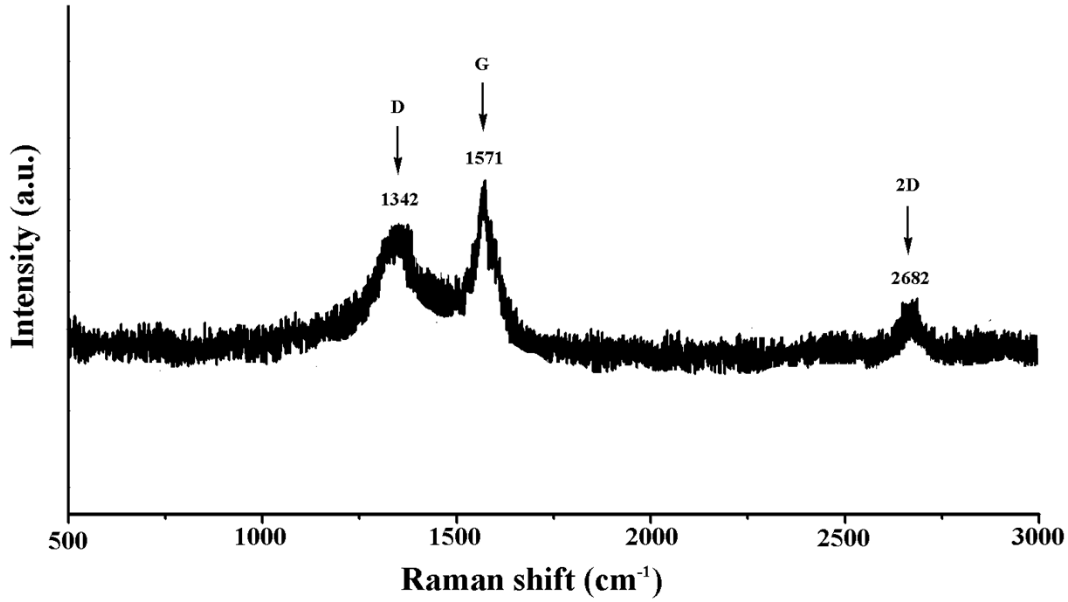

Fig. S12 Raman spectrum (λ_{ex} = 514.5 nm, 0.4 mW) of the graphene.

(a)

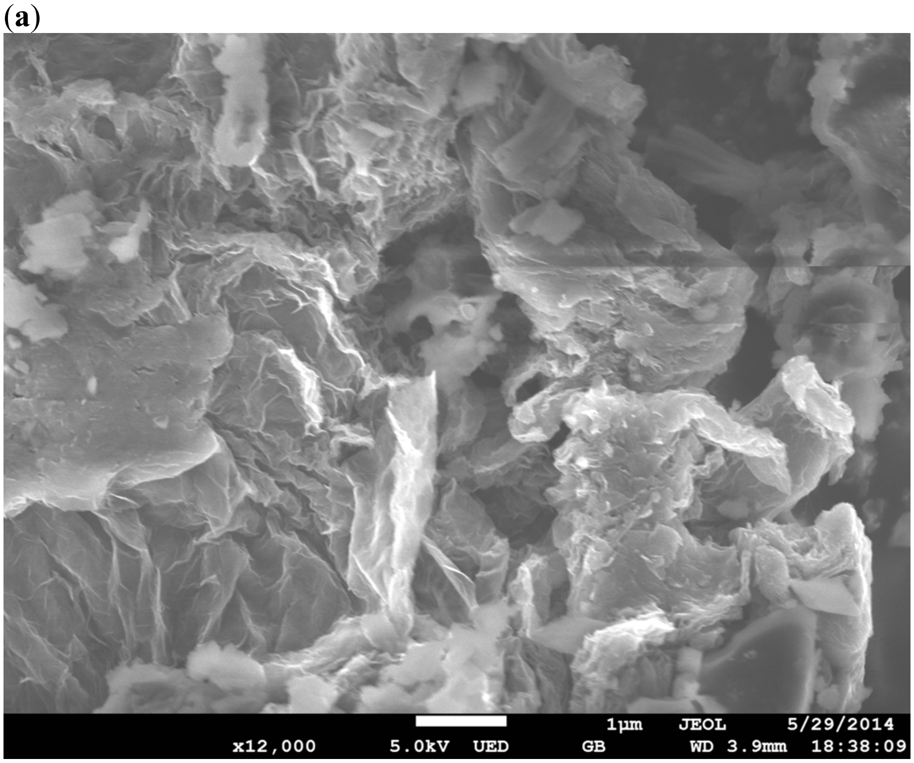

(**b**)

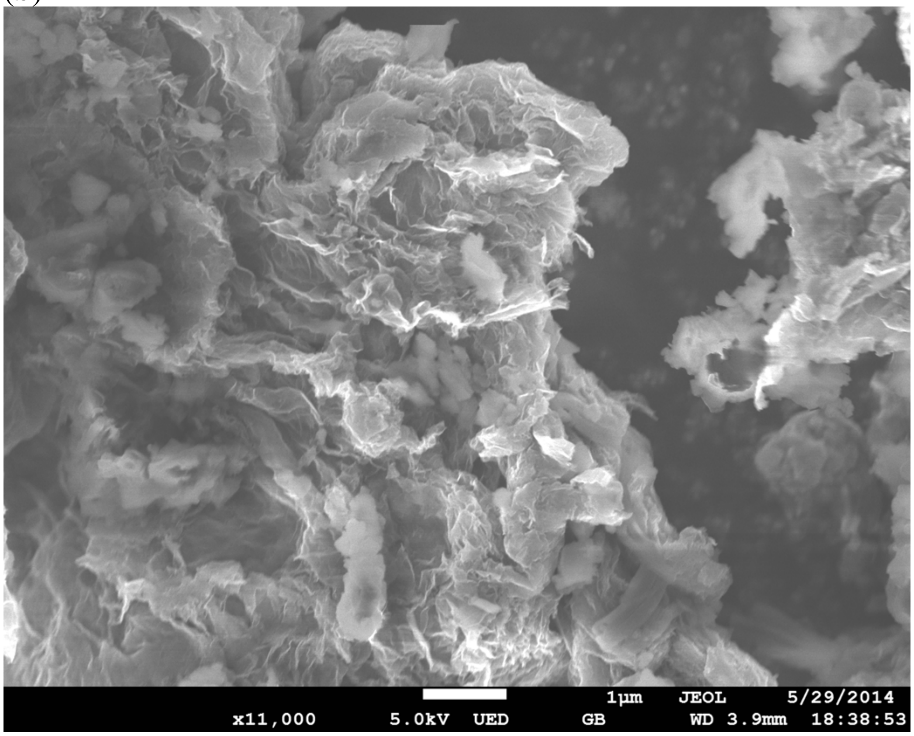

(**c**)

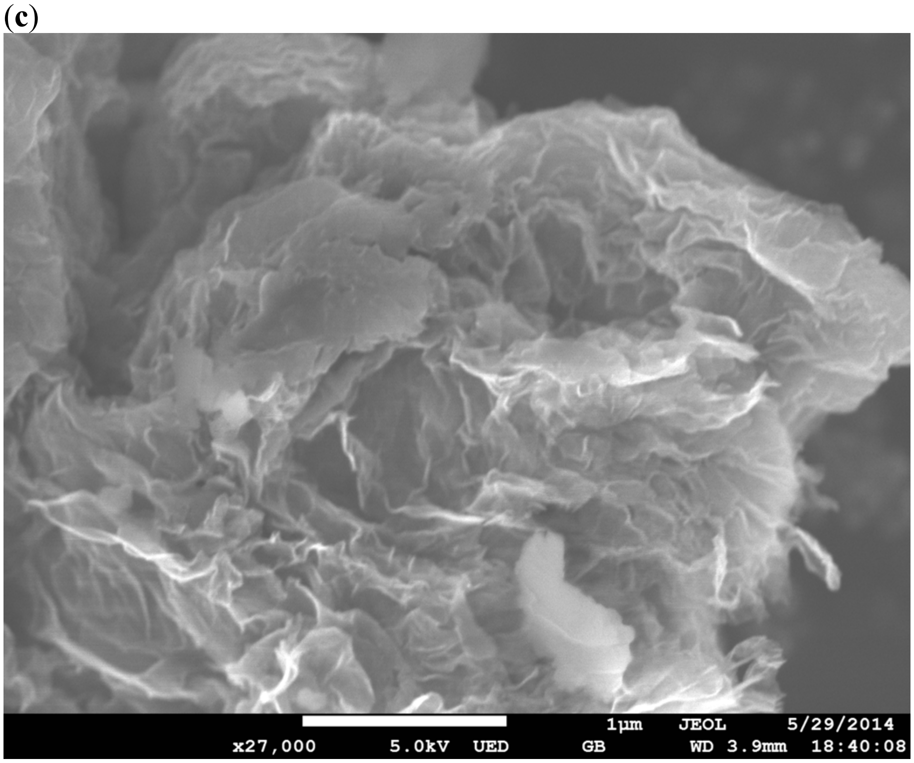

Fig. S13 SEM images of the complex **1**/graphene composite.

(**a**)

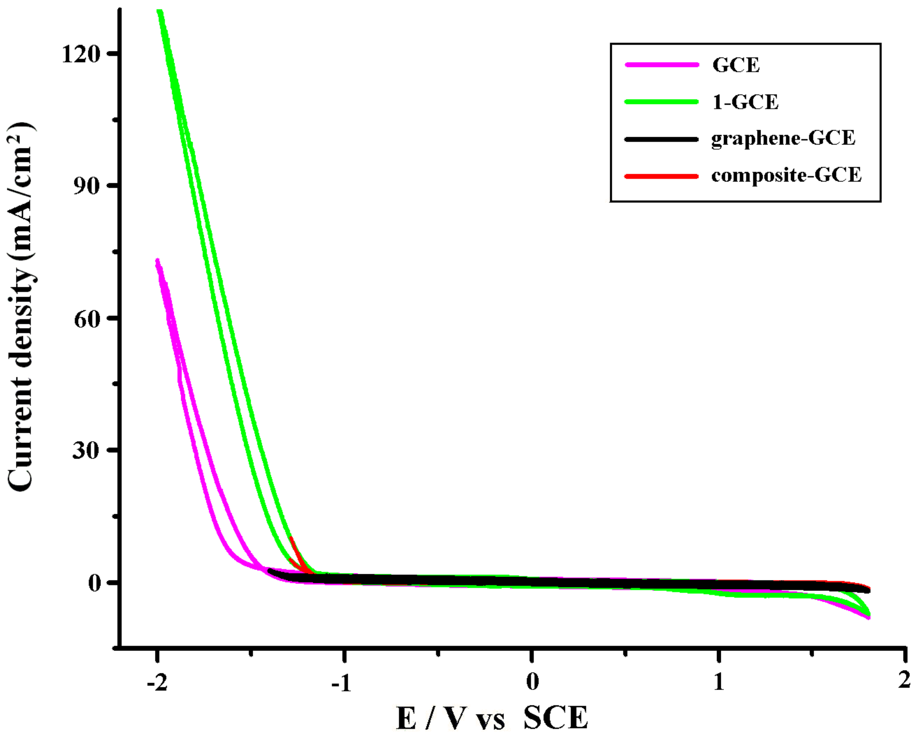

(**b**)

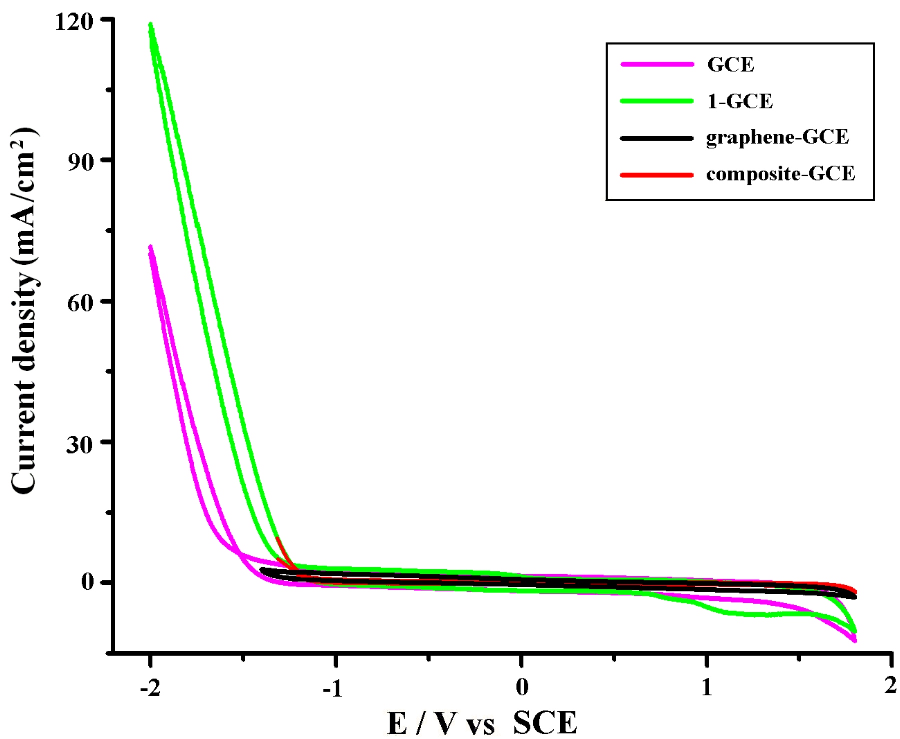

Fig. S14 CVs of the bare **GCE**, **1-GCE, graphene-GCE** and **composite-GCE** in 0.5 M Na_2SO_4 solution (50mL) at a sweep rate of 20 (**a**) and 50 mV·s^{-1} (**b**).

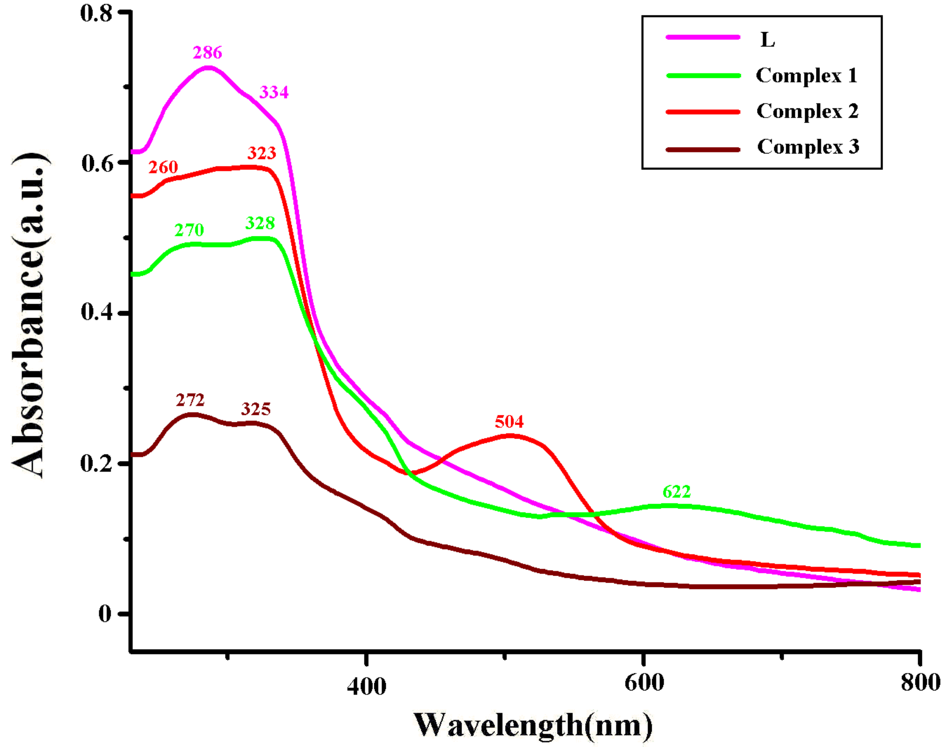

Fig. S15 UV-vis absorption spectra at room temperature for the free organic ligand **L** and complexes **1-3**.

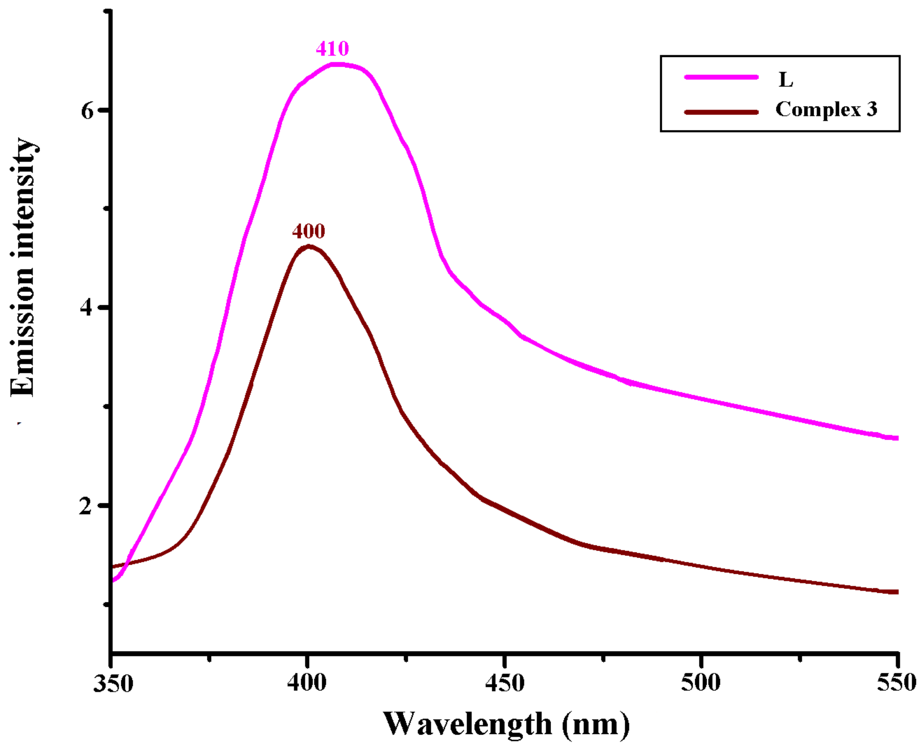

Fig. S16 Solid-state emission spectra at room temperature for the free ligand **L** and complex **3**.

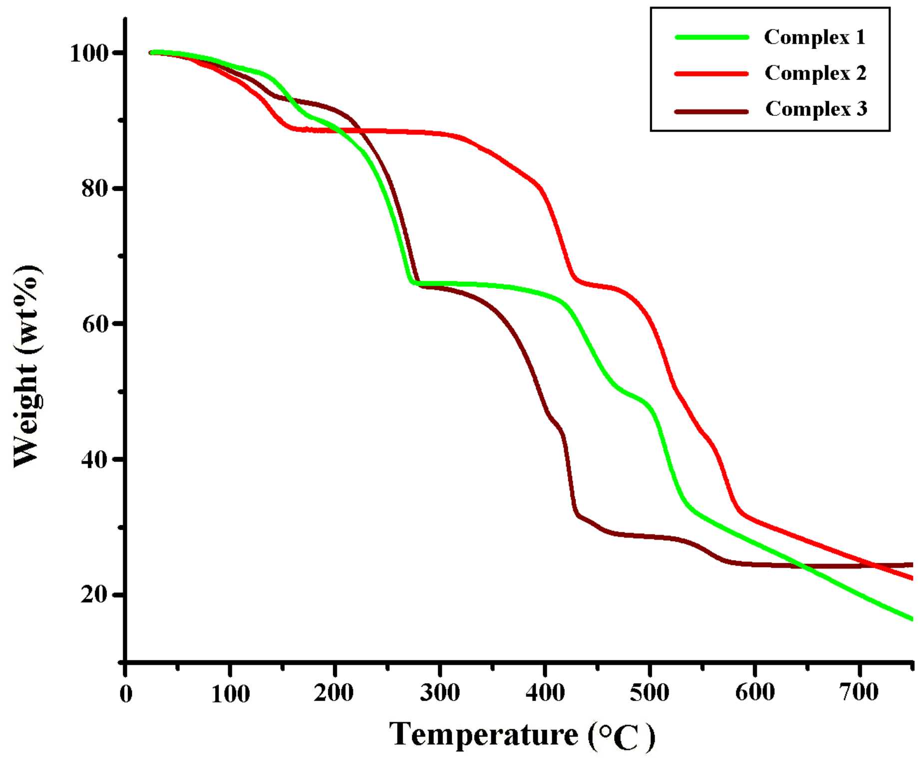

Fig.S17 Thermogravimetric curves of complexes **1** (green), **2** (red) and **3** (brown).

References:

1 Y. J. Sun, J. P. Bigi, N. A. Piro, M. L. Tang, J. R. Long and C. J. Chang, *J. Am. Chem. Soc.*, **2011**, *133*, 9212.